PHYSICAL REVIEW B **88**, 094437 (2013)

Chiral properties of hematite α-Fe_2O_3 inferred from resonant Bragg diffraction using circularly polarized x rays

A. Rodríguez-Fernández,[1] J. A. Blanco,[1] S. W. Lovesey,[2] V. Scagnoli,[3] U. Staub,[3] H. C. Walker,[4]
D. K. Shukla,[4,*] and J. Strempfer[4]
[1]*Departamento de Física, Universidad de Oviedo, E-33007 Oviedo, Spain*
[2]*ISIS Facility and Diamond Light Source Ltd, Oxfordshire OX11 0QX, United Kingdom*
[3]*Paul Scherrer Institut, 5232 Villigen, Switzerland*
[4]*Deutsches Elektronen-Synchrotron, 22607 Hamburg, Germany*

(Received 20 June 2013; revised manuscript received 21 August 2013; published 26 September 2013)

Chiral properties of the two phases—collinear motif (below Morin transition temperature, $T_M \approx 250$ K) and canted motif (above T_M)—of magnetically ordered hematite (α-Fe_2O_3) have been identified in single-crystal resonant x-ray Bragg diffraction using circular polarized incident x rays tuned near the iron K edge. Magnetoelectric multipoles, including an anapole, fully characterize the high-temperature canted phase, whereas the low-temperature collinear phase supports both parity-odd and parity-even multipoles that are time odd. Orbital angular momentum accompanies the collinear motif, whereas it is conspicuously absent with the canted motif. Intensities have been successfully confronted with analytic expressions derived from an atomic model fully compliant with chemical and magnetic structures. Values of Fe atomic multipoles previously derived from independent experimental data are shown to be completely trustworthy.

DOI: 10.1103/PhysRevB.88.094437 PACS number(s): 78.70.Ck, 78.20.Ek, 75.50.Ee, 75.47.Lx

I. INTRODUCTION

Alpha ferric oxide (α-Fe_2O_3), also known as hematite, a name deriving from the Greek "$\alpha\iota\mu\alpha\tau\iota\tau\eta\varsigma$" due to its bloodlike shade in powder form, is still today revealing its mysteries.[1,2] Hematite has been present in the scientific literature since the studies performed by the Greek philosopher Theophrastus around 315 B.C. and later was studied by the father of magnetism, William Gilbert of Colchester, in the 16th century. Its magnetic behavior was first studied in the early 20th century by Honda and Soné (1914), but it was not until Dzyaloshinsky in 1958 when it was defined as a canted antiferromagnet, becoming the prototype of the Dzyaloshinsky-Moriya interaction.[3,4]

Hematite is a member of the corundum-structure family (centrosymmetric space group 167, $R\bar{3}c$). The ferric (Fe^{3+}, $3d^5$) ions present in α-Fe_2O_3 are arranged along the c axis occupying 4(c) sites, and they occupy sites deprived of spatial inversion symmetry. The resonant x-ray diffraction data we present in this paper are witness to the absence of local inversion symmetry in the presence of global inversion symmetry. The antiferromagnetic behavior present in this compound below its Néel temperature ($T_N \approx 948$ K) shows two different magnetic orders separated by the Morin transition temperature, $T_M \approx 250$ K. Below this temperature the magnetic moments are all parallel to the hexagonal c axis in a collinear antiferromagnetic G-type configuration (that is, the nearest neighbors have opposite spins while the next-nearest neighbors have parallel spins) with an iron magnetic moment of $4.9\mu_B$ at 77 K, while above T_M the material shows a magnetic motif where the moments are in a (basal) plane normal to the c axis showing a canted antiferromagnetic order, depicted in Fig. 1. As previously, we follow Dzyaloshinsky and label the collinear (low-temperature phase) and canted (room-temperature phase) magnetic motifs as I and II, respectively.[5] The Dzyaloshinsky-Moriya antisymmetric interaction is responsible for the behavior known as weak ferromagnetism that in the case of hematite is parallel to the dyad axis of rotational symmetry.[1,3]

Chiral order in electronic structure is unambiguously detected by a probe with a matching characteristic, as discussed by Rodríguez-Fernández*et al.*,[6] and we have used circularly polarized x rays to verify the existence of such order in a single crystal of hematite. With respect to the chirality, neutrons have perhaps given the clearest indication of such states in the past. However, the method of determining this also involves measuring the polarization of the scattered neutrons,[7] and in this case, where there is a net ferromagnetic contribution in the high-temperature phase of α-Fe_2O_3, the neutron method cannot be used because the ferromagnetic component will depolarize the incident neutrons. In contrast, tuning the x-ray energy to an atomic resonance of a ferric ion, the Fe K edge, means these ions and no others participate in the chiral order observed. In addition, the resonant process enhances the sensitivity of the scattering process to the local environments and angular anisotropy in the electron distribution that appears due to the spin, charge, or multipolar order.[5,6,8–13]

Previous experiments on hematite, using Bragg diffraction of linearly polarized x rays with the primary energy tuned near the iron K absorption edge, were performed by Finkelstein *et al.* and Kokubun *et al.*[14,15] Owing to the important contribution of the Thomson scattering in these types of experiments, attention is given to Bragg reflections that are space-group forbidden by extinction rules. Integer Miller indices obey the extinction rule l odd and $-h + k + l = 3n$ in the case of hematite.

Finkelstein *et al.* observed,[14] while rotating a single crystal about the Bragg wave vector $(003)_H$ in a so-called azimuthal-angle scan, a sixfold periodicity of the intensity that is traced to a triad axis of rotational symmetry that passes through sites occupied by resonant, ferric ions. At a later date, Kokubun *et al.* reported azimuthal-angle scans for $l = 3$ and 9.[15] Unlike these two groups, we exploit the polarization analysis of the diffracted beam to unveil contributions to the

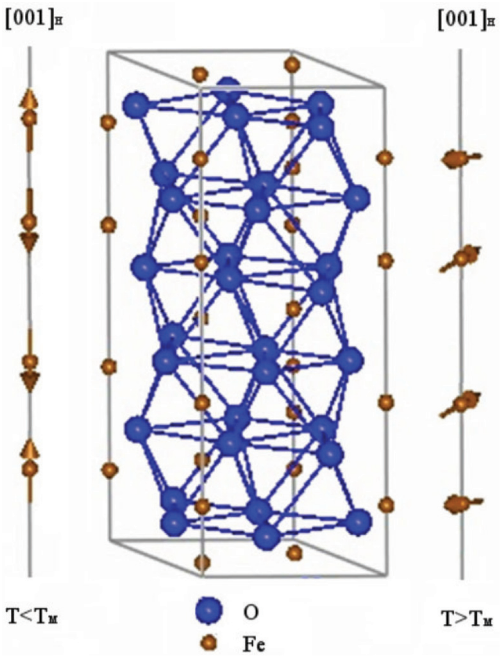

FIG. 1. (Color online) Crystal and magnetic structure of hematite. The small orange dots represent ferric ions while the large blue dots present the oxygen atoms' positions. The vertical line at left denotes the magnetic motif along the *c* axis below the Morin temperature (phase I). The vertical line at right denotes the motif above the Morin temperature, where iron moments are contained in the *a*-*b* plane (phase II).

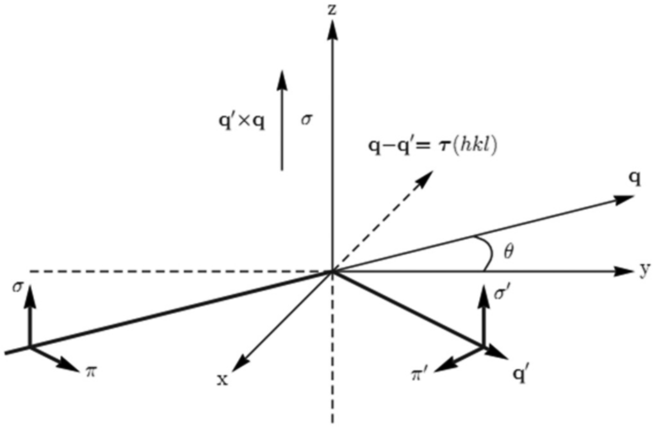

FIG. 2. Cartesian coordinates (x,y,z) and x-ray polarization and wave vectors. The plane of scattering spanned by primary ($\mathbf{q}$) and secondary ($\mathbf{q}'$) wave vectors coincides with the x-y plane. Polarization labeled σ and σ' is normal to the plane and parallel to the z axis, while polarization labeled π and π' lies in the plane of scattering. The beam is deflected through an angle of 2θ.

magnetization with different spatial symmetries. On the way, we confirm our prediction that hematite supports chiral order[5] and gain confidence in our previously reported values of Fe atomic multipoles, because they provide a totally satisfactory description of new azimuthal-angle data for $l = 3$ and 9 gathered in phase I and phase II. A potential uncertainty in our analysis[5] of data reported in Ref. 15 is set to rest. Previously, we were forced to the conclusion that there is an error in Ref. 15 on the reported setting of the crystal in azimuthal-angle scans, and the error is confirmed here by use of our own data.

In this paper, we present data from a circular polarized x-ray diffraction experiment performed at the Fe K edge. Section II contains the description of the crystal and experiment. This is followed by the discussion of the results in Sec. III, where we report a detailed analysis of our azimuthal-angle scans for $l = 3$ and 9, for the hematite sample at 150 K (collinear motif, phase I) and 300 K (canted motif, phase II). In Sec. IV we present our final remarks and conclusions.

II. CRYSTAL AND EXPERIMENTAL METHOD

The synthetic hematite single crystal studied in this experiment was purchased from the Mateck Company. The size of the sample was about 10 × 10 mm^2 with a thickness of 0.5 mm, showing a polished surface near the $[00l]_H$ direction. In Cartesian coordinates our hexagonal crystal coordinates are $a_H = a(1,0,0)$, $b_H = a(-1/2,\sqrt{3}/2,0)$, and $c_H = c(0,0,1)$, with $a = 5.038$ Å and $c = 13.712$ Å.

The experimental data presented in this work were obtained at the Beamline P09, located in the synchrotron source PETRA III (Germany).[16] This beam line covers the energy range from 2.7 to 24 keV. A double-phase-retarder setup is used to obtain the circular and rotated linear polarization for the incident beam. The double-phase-retarder setup corrects for some depolarizing effects and accomplishes a better rotated polarization rate.[17–19] Details of the incident polarization manipulation using diamond phase plates at P09 are described elsewhere.[16,17] The phase plates are followed by a focusing and higher-harmonic rejection system consisting of vertically reflecting mirrors. The plate-shaped crystal, attached to the cold finger of a closed-cycle cryostat, was mounted on a Psi diffractometer such that the $[00l]_H$ direction of the crystal is parallel to the scattering vector, $\mathbf{q} - \mathbf{q}'$, as shown in Fig. 2. Polarization analysis was performed using a Cu(220) analyzer crystal. The states of polarization labeled π (π') and σ (σ') are defined in Fig. 2.

In the case of $R\bar{3}c$, the reflections $(003)_H$ and $(009)_H$ are space-group forbidden, but weak Bragg diffraction occurs near an atomic resonance, as demonstrated by data displayed in Fig. 3. In the experiment performed at Beamline P09, the energy at which the primary x-ray beam was tuned, 7115 eV, is close to the iron K edge. At this energy the forbidden $(003)_H$ and $(009)_H$ reflections were investigated with the sample maintained at two different temperatures, below (150 K) and above (300 K) the Morin temperature.

During the experiment the incident polarization was switched between almost perfect right and left circular polarization. A measure of the high quality of circular polarization of the primary beam is demonstrated by small values of the parameters for linear polarization (following the convention of Pauli matrices as done by Lovesey *et al.*), namely, $P_1 = 0.010 \pm 0.002$ and $P_3 = 0.026 \pm 0.002$ for right handed, and $P_1 = -0.016 \pm 0.002$ and $P_3 = 0.036 \pm 0.002$ for left handed. (Properties of Stokes parameters are mentioned again in Sec. III.[20,21])

We have found an extensive contribution from Renninger reflections, also known as multibeam reflections. The subtraction of this kind of background intensity was done using

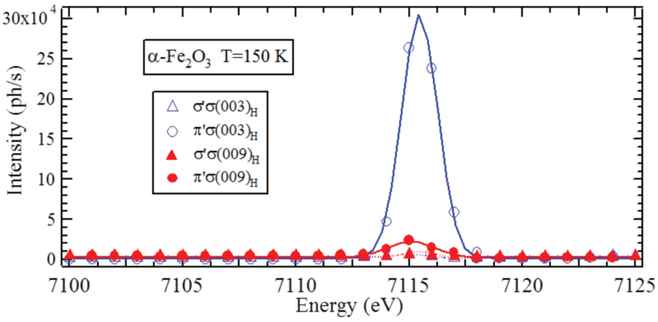

FIG. 3. (Color online) X-ray energy dependence below T_M $T = 150$ K for both reflections $(003)_H$ and $(009)_H$ in the vicinity of the iron K edge. The open blue circles (triangles) show the linear polarized $\pi'\sigma$ $(\sigma'\sigma)$ data for the $(003)_H$ reflection, while the red circles (triangles) define the data from the $\pi'\sigma$ $(\sigma'\sigma)$ polarized channel for the $(009)_H$ reflection. The solid lines present the fitting to a model of a single oscillator.

a MATLAB program developed by Nisbet as previously done for the extraction of the data presented in Ref. 6. Attention was focused on azimuthal angles either only lightly or not contaminated by Renninger reflections (therefore, measured points in the azimuth dependence are not equidistant).

Circular left (C_L) and circular right (C_R) polarized azimuthal scans were performed at room temperature; the difference between these two polarizations is presented in Fig. 4. Fitting to data above T_M was performed using Eqs. (3) and (4) presented in Sec. III. The multipole values used for these fittings are shown in Table I (phase II) and they agree with the ones derived by Lovesey *et al.*[5]

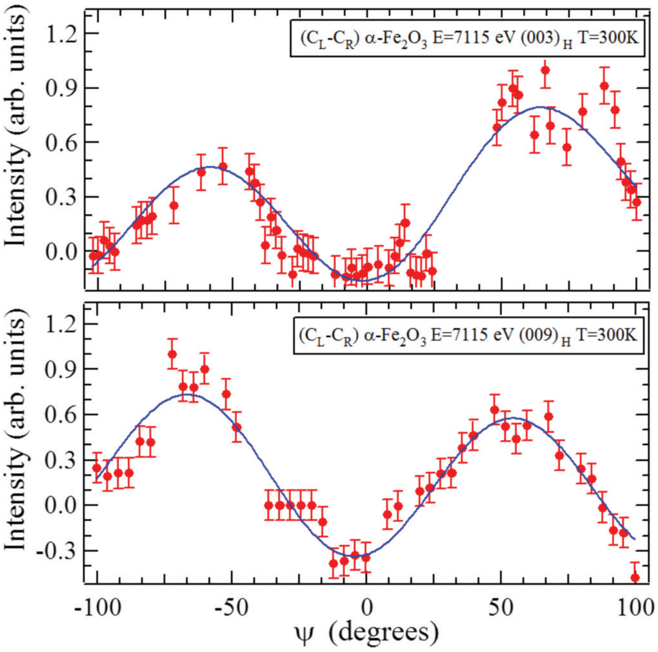

FIG. 4. (Color online) Azimuthal-angle scans for phase II (canted motif) at 300 K. Difference between circular left (C_L) and circular right (C_R) polarization for the $(003)_H$ reflection (top) and the $(009)_H$ reflection (bottom). The red circles represent the experimental data while the blue line shows expression (5) for pure $E1$-$E2$ resonance evaluated with multipoles taken from Ref. 5 and reproduced in Table I.

TABLE I. Numerical values of multipoles reported in Ref. 5 and used here for intensities generated from expressions (3)–(6). As in Ref. 5, $\langle T^4_3\rangle'$ and $\langle U^2_0\rangle$, multipoles which contribute in both phases, are fixed to 10 and 0.5, respectively.

Multipole	Phase I	Phase II
$\langle G^1_{+1}\rangle'$		$5.0(2)\times 10^{-1}$
$\langle G^2_{+1}\rangle''$		$-3.8(3)\times 10^{-1}$
$\langle G^3_{+1}\rangle'$		$10.7(6)\times 10^{-1}$
$\langle G^3_{+3}\rangle'$	$4.1(2)\times 10^{-1}$	$24.5(5)\times 10^{-1}$
$\langle T^3_3\rangle''$	$1.0(1)\times 10^{-4}$	

The azimuthal scan dependence of the $(003)_H$ reflection below T_M is presented in Fig. 5, whereas that for the $(009)_H$ reflection is shown in Fig. 6. As in the case of room temperature, multipole values used in the fitting are those derived by Lovesey *et al.*, collected in Table I (phase I).[5]

III. RESULTS AND DISCUSSION

For an interpretation of the experimental data, shown in Figs. 4, 5, and 6, we proceed as in Ref. 5. The contribution of Thomson scattering is absent at space-group-forbidden reflections, leaving a sum of nonresonant spin and a resonant contribution as ingredients for the appropriate scattering amplitude.[21,22]

The spin contribution, G^s, is explicitly first order in the small quantity E/mc^2, where E is the primary energy and mc^2 the electron rest mass energy. Using notation displayed in Fig. 2, $G^s = i(E/mc^2)(\mathbf{e}\times\mathbf{e}')\cdot\,\mathbf{F_s}(\mathbf{k})$, where $\mathbf{k}=\mathbf{q}-\mathbf{q}' = (h,k,l)$ and $\mathbf{e}$ and $\mathbf{q}$ ($\mathbf{e}'$ and $\mathbf{q}'$) are, respectively, the polarization vector and wave vector of the primary (secondary) photon, while $\mathbf{F_s}(\mathbf{k})$ is the unit-cell structure factor for spin dipoles.[23,24]

The measured energy profiles, displayed in Fig. 3 for the reflections $(003)_H$ and $(009)_H$, show a single resonance in the pre-edge region that can be adequately modeled by a single

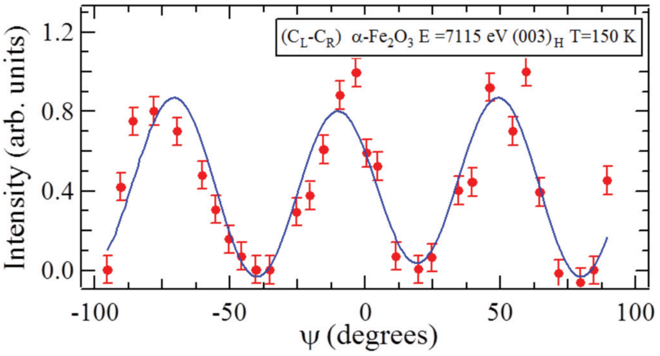

FIG. 5. (Color online) Azimuthal-angle scan for phase I (collinear motif) at 150 K. Difference between circular left (C_L) and circular right (C_R) polarization for $(003)_H$ reflection. The red circles represent the experimental data while the blue line shows expressions (3) and (4) for a mixture of $E1$-$E2$ and $E2$-$E2$ resonances evaluated with multipoles taken from Ref. 5 and reproduced in Table I. In Eq. (4) the parity-even and time-odd octupole $\langle T^3_3\rangle''$ is given a nominal value of $1(\pm 0.1)\times 10^{-4}$.

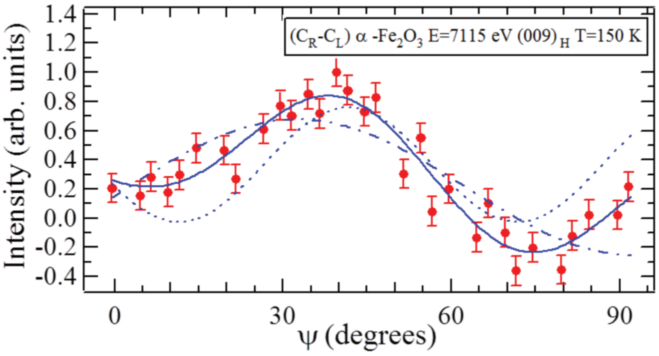

FIG. 6. (Color online) Azimuthal-angle scan for phase I (collinear motif) at 150 K. Difference between circular left (C_L) and circular right (C_R) polarization for the $(009)_H$ reflection. As in Fig. 5, the red circles represent the experimental data while the blue line shows a mixture of $E1$-$E2$ and $E2$-$E2$ resonances. Data are compared to pure $E1$-$E2$ [Eq. (3)] (dashed line) and pure $E2$-$E2$ [Eq. (4)] (dotted line) resonances, with multipoles taken from Ref. 5 and reproduced in Table I. In Eq. (4) the octupole $\langle T^3_3\rangle''$ is given a nominal value of 0.0001.

oscillator centered at an energy $\Delta = 7115$ eV.[5] The resonant contribution to scattering is represented by $d(E)F_{\mu'\nu}$, where $d(E) = \Delta/[E - \Delta + i\Gamma]$ with Γ the width in energy and $F_{\mu'\nu}$ a unit-cell structure factor for states of polarization μ' (secondary) and ν (primary), as in Fig. 2.

The generic form of our Bragg scattering amplitude for hematite at a space-group-forbidden reflection (no Thomson scattering) is

$$G_{\mu'\nu}(E) = G^s_{\mu'\nu} + \rho d(E)F_{\mu'\nu}. \qquad (1)$$

In this expression, ρ is a collection of factors, which includes radial integrals for particular resonance events, namely, $\rho(E1\text{-}E1) = [\{R\}_{sp}/a_o]^2\aleph$, $\rho(E1\text{-}E2) = [q\{R^2\}_{sd}\{R\}_{sp}/a_o^2]\aleph$, and $\rho(E2\text{-}E2) = [q\{R^2\}_{sd}/a_o]^2\aleph$. Here, $\aleph$ is a dimensionless quantity related to the Bohr radius a_0 and the resonant energy $\Delta = 7115$ eV, with $\aleph = m\Delta a_o^2/\hbar^2 = 260.93$. The sizes of radial integrals for the $E1$ and $E2$ processes at the K absorption edge, $\{R\}_{sp}$ and $\{R^2\}_{sd}$, are discussed in Ref. 5.

The polarization state of the photons, already briefly discussed in Sec. II, is defined by Stokes parameters that are purely real and time even, namely, ordinary scalars P_1 and P_3 for linear polarization, and a pseudoscalar P_2 that represents the helicity of the beam. The contribution to the total intensity induced by circular polarization (helicity), I_c, is[20]

$$I_c = P_2 \,\mathrm{Im}\,\{G^*_{\sigma'\pi}\, G_{\sigma'\sigma} + G^*_{\pi'\pi}\, G_{\pi'\sigma}\}, \qquad (2)$$

where the amplitudes $\mathrm{G}_{\mu'\nu}$ are given by Eq. (1) and * denotes complex conjugation. I_c is zero for Thomson scattering since it is proportional to $(\mathbf{e}\cdot\mathbf{e}')$ and diagonal with respect to the polarization states.

We make use of unit-cell structure factors reported in our previous publication.[5] Full use is made of the established chemical and magnetic structures in their construction. Degrees of freedom in the electronic ground state of a ferric ion are captured in atomic multipoles labeled by their rank, K, and projection, $Q(-K \leqslant Q \leqslant K)$.[21,22] Two types of multipoles are required, parity even, $\langle T^K_Q\rangle$, and two flavors of parity-odd multipoles, $\langle G^K_Q\rangle$ and $\langle U^K_Q\rangle$, distinguished by their time signatures. Magnetoelectric multipoles, $\langle G^K_Q\rangle$, are time odd and absent in the paramagnetic phase, and polar multipoles, $\langle U^K_Q\rangle$, are time even, while $(-1)^K$ is the time signature of $\langle T^K_Q\rangle$. Parity-even multipoles arise in $E1$-$E1$ and $E2$-$E2$ resonant events, and parity-odd multipoles are required for $E1$-$E2$ events, where $E1$ denotes an electric-dipole operator and $E2$ denotes an electric-quadrupole operator. All multipoles have the complex conjugate $\langle O^K_Q\rangle^* = (-1)^Q\ \langle O^K_{-Q}\rangle$, with $\langle O^K_0\rangle$ purely real, and the relative phase of real and imaginary components is set by $\langle O^K_Q\rangle = \langle O^K_Q\rangle' + i\langle O^K_Q\rangle''$.

Expressions for I_c given in Ref. 5 are repeated here for the convenience of the reader.

Below T_M (phase I, collinear motif). There is no contribution to I_c from $E1$-$E1$ reflection, due to crystal symmetry, and

$$I_c(E1\text{-}E2) = -P_2\left(\frac{8\sqrt{2}}{5}\right)\rho^2(E1\text{-}E2)|d(E)|^2\sin(3\psi) \times \cos^3(\theta)\,[1+\sin^2(\theta)]\cos^2(\varphi l)\langle G^3_{+3}\rangle'\langle U^2_0\rangle, \qquad (3)$$

$$I_c(E2\text{-}E2) = -P_2\, 4\rho^2(E2\text{-}E2)|d(E)|^2\sin(6\psi) \times \sin(\theta)\cos^6(\theta)\sin^2(\varphi l)\langle T^3_{+3}\rangle''\langle T^4_{+3}\rangle'. \qquad (4)$$

In these expressions, the angle $\varphi = -\pi u$, where $u = 2z - 1/2 = 0.2104$ for α-Fe$_2$O$_3$.

At the K edge, when the spin degrees of freedom associated with the resonant ion are absent in the electronic ground state, the parity even multipoles with K odd are function only of the orbital angular momentum.[25] In this case, $\langle T^3_3\rangle''$ in Eq. (4) is zero for the pure ferric ion, because it has a shell that is half filled and spherically symmetric (^{6}S, $3d^5$). In our previous study, where we interpreted data published by Kokubun *et al.*,[15] we took $\langle T^3_3\rangle'' = 0$ on this basis. Our superior data displayed in Figs. 5 and 6, collected with the benefit of polarization analysis, shows that $\langle T^3_3\rangle''$ is different from zero in Eq. (4). As a consequence, the ferric ion possesses unquenched orbital angular momentum.

Dashed and dotted lines in Fig. 6 show our data for the $(009)_H$ reflection compared separately to $E1$-$E2$ and $E2$-$E2$ reflections. Evidently, a single event is not responsible for our observed intensities. However, a combination of the two events, $E1$-$E2$ and $E2$-$E2$, provides a satisfactory account; the fit represented by the continuous line in Fig. 6 confirms that this is so.

Concerning the contribution to the intensity from parity-odd multipoles [Eq. (3)], the requirement to have a value different from zero tells us that $(\langle G^3_3\rangle', \langle U^2_0\rangle)$ is not zero. Notably, $\langle U^2_0\rangle$ is a manifestation of local chirality.[21,22,25,26] The polar quadrupole is the same in the two phases, because it is related to chemical structure, whereas $\langle G^3_3\rangle'$ has a similar, small value in phase I and a much larger value in phase II.

Above T_M (phase II, canted motif). Our data for this phase and two reflections are displayed in Fig. 4. Appropriate expressions for intensities induced by circular polarization in the primary beam are[5]

$$I_c(E1\text{-}E2) = P_2\left(\frac{8\sqrt{2}}{5}\right)\rho^2(E1\text{-}E2)\,|d(E)|^2\cos^2(\varphi l)\cos^2(\theta)\langle U_0^2\rangle\left\{\frac{1}{\sqrt{3}}\sin(\psi)\left[\frac{-3}{\sqrt{5}}[\cos(3\theta)+\cos(\theta)]\langle G_{+1}^1\rangle' + [\cos(3\theta) - \cos(\theta)]\,\langle G_{+1}^2\rangle'' - \frac{1}{\sqrt{5}}\,[\cos^3(\theta)+2\cos(\theta)]\langle G_{+1}^3\rangle'\right] - \sin(3\psi)\cos(\theta)\,[1+\sin^2(\theta)]\langle G_{+3}^3\rangle'\right\}, \tag{5}$$

$$I_c(E2\text{-}E2) = -P_2\left(\frac{1}{\sqrt{2}}\right)\rho^2(E2\text{-}E2)|d(E)|^2\sin^2(\varphi l)\langle T_{+3}^4\rangle'\left\{4\sin(\psi)\cos^4(\theta)\left[\frac{-1}{\sqrt{5}}\sin(\theta)\,[8\cos^2(\theta)-5]\langle T_1^1\rangle'' + \sqrt{\frac{3}{5}}\sin(\theta)\cos^3(\theta)\langle T_{+1}^3\rangle''\right] - 4\sqrt{2}\sin(\theta)\cos^6(\theta)\sin(6\psi)\,\langle T_{+3}^3\rangle''\right\}. \tag{6}$$

Our data in Fig. 4 agree with the prediction of an $E1$-$E2$ event [Eq. (5)] evaluated with multipoles carried over from our previous work.[5] Correspondingly, magnetoelectric multipoles are large compared to their values in phase I, with an octupole dominant. Treating $\langle T_Q^K\rangle$ with K odd in Eq. (6) as unknowns, it is not possible to find a satisfactory fit to a pure $E2$-$E2$ event, and it has no role in an interpretation of phase II. As the hexadecapole $\langle T_3^4\rangle'$ is the same in the two phases, because it is determined by chemical structure, and likewise local chirality $\langle U_0^2\rangle$, we conclude that orbital angular momentum, manifest through $\langle T_Q^K\rangle$ with K odd, is insignificant in the high-temperature magnetic phase.

IV. CONCLUSION

We report extensive data on magnetically ordered hematite gathered with the experimental technique of x-ray Bragg diffraction augmented by an atomic resonance. The primary energy was tuned close to the iron K edge, and intensities were measured at space-group-forbidden reflections, $(003)_H$ and $(009)_H$, that are exceptionally sensitive to magnetic degrees of freedom in the electronic ground state. The use of polarization analysis improved the quality of our data significantly. We chose circular polarization and reported differences in intensities gathered with left- and right-handed primary polarization.

The existence of intensity induced by circular polarization confirms that magnetically ordered hematite is chiral, as we predicted.[5] Moreover, we confirm that our previous estimates of parity-odd multipoles, using data published by Kokubun *et al.*,[15] are completely trustworthy. Below the Morin transition, the collinear motif contains orbital angular momentum and the ferric ion is not spherically symmetric (e.g., ^6S, $3d^5$). However, we find no evidence of orbital angular momentum in the canted motif that exists above the Morin transition. In this phase, diffraction can be interpreted with parity-odd multipoles only, with magnetoelectric octupoles making the dominant contribution. The existence of an orbital magnetic moment is a consequence of the spin-orbit coupling, which is a necessary ingredient of the Dzyaloshinsky-Moriya interaction that is responsible for the noncollinear magnetic structure above T_M. However, the magnitude of the orbital magnetic moment at room temperature is almost negligible compared to that found at 150 K, owing to entropic effects where the orientation of the orbital moment is almost randomized by its thermal energy. Additional experiments at intermediate temperatures could confirm this issue.

ACKNOWLEDGMENTS

Financial support has been received from Spanish FEDER-MiCiNN Grant No. MAT2011-27573-C04-02. One of us (A.R.F.) is grateful to Gobierno del Principado de Asturias for the financial support from Plan de Ciencia, Tecnología e innovación (PTCI) de Asturias. We thank the Deutsches Elektronen-Synchrotron for access to Beamline P09 of the synchrotron PETRA III (I-20110433 EC) that contributed to the results presented here. This work has been supported by National Centre of Competence of Research—Materials with Novel Electrical Properties of the Swiss National Science Foundation.

---

[*] Present address: UGC DAE Consortium for Scientific Research, Khandwa Road, Indore 01, India.

[1] A. H. Morrish, *Canted Antiferromagnetism: Hematite* (World Scientific, Singapore, 1994).

[2] M. Catti, G. Valerio, and R. Dovesi, Phys. Rev. B **51**, 7441 (1995).

[3] I. Dzyaloshinsky, J. Phys. Chem. Solids **4**, 241 (1958).

[4] T. Moriya, Phys. Rev. **120**, 91 (1960).

[5] S. W. Lovesey, A. Rodríguez-Fernández, and J. A. Blanco, Phys. Rev. B **83**, 054427 (2011).

[6] A. Rodríguez-Fernández, S. W. Lovesey, S. P. Collins, G. Nisbet, and J. A. Blanco, arXiv:1305.0484 [cond-mat.mtrl-sci].

[7] J. A. Blanco, P. J. Brown, A. Stunault, K. Katsumata, F. Iga, and S. Michimura, Phys. Rev. B **73**, 212411 (2006).

[8] S. W. Lovesey and V. Scagnoli, J. Phys.: Condens. Matter **21**, 474214 (2009).

[9] J. Fernández-Rodríguez, J. A. Blanco, P. J. Brown, K. Katsumata, A. Kikkawa, F. Iga, and S. Michimura, Phys. Rev. B **72**, 052407 (2005).

[10] S. W. Lovesey, J. Fernández-Rodríguez, J. A. Blanco, D. S. Sivia, K. S. Knight, and L. Paolasini, Phys. Rev. B **75**, 014409 (2007).

[11] S. B. Wilkins, R. Caciuffo, C. Detlefs, J. Rebizant, E. Colineau, F. Wastin, and G. H. Lander, Phys. Rev. B **73**, 060406 (2006).

[12] J. A. Paixão, C. Detlefs, M. J. Longfield, R. Caciuffo, P. Santini, N. Bernhoeft, J. Rebizant, and G. H. Lander, Phys. Rev. Lett. **89**, 187202 (2002).
[13] Y. Tanaka, T. Inami, S. W. Lovesey, K. S. Knight, F. Yakhou, D. Mannix, J. Kokubun, M. Kanazawa, K. Ishida, S. Nanao, T. Nakamura, H. Yamauchi, H. Onodera, K. Ohoyama, and Y. Yamaguchi, Phys. Rev. B **69**, 024417 (2004).
[14] K. D. Finkelstein, Q. Shen, and S. Shastri, Phys. Rev. Lett. **69**, 1612 (1992).
[15] J. Kokubun, A. Watanabe, M. Uehara, Y. Ninomiya, H. Sawai, N. Momozawa, K. Ishida, and V. E. Dmitrienko, Phys. Rev. B **78**, 115112 (2008).
[16] J. Strempfer, S. Francoual, D. Reuther, D. K. Shukla, A. Skaugen, H. Schilte-Schrepping, T. Kracht, and H. Franz, J. Synchrotron Rad. **20**, 541 (2013).
[17] S. Francoual, J. Strempfer, D. Reuther, D. K. Shukla, and A. Skaugen, J. Phys. Conf. Ser. **425**, 132010 (2013).
[18] K. Okitsu, Y. Ueji, K. Sato, and Y. Amemiya, J. Synchrotron Radiat. **8**, 33 (2001).
[19] V. Scagnoli, C. Mazzoli, C. Detlefs, P. Bernard, A. Fondacaro, L. Paolasini, F. Fabrizi, and F. de Bergevin, J. Synchrotron Radiat. **16**, 778 (2009).
[20] J. Fernández-Rodríguez, S. W. Lovesey, and J. A. Blanco, Phys. Rev. B **77**, 094441 (2008).
[21] S. W. Lovesey, E. Balcar, K. S. Knight, and J. Fernández-Rodríguez, Phys. Rep. **411**, 233 (2005).
[22] S. W. Lovesey and E. Balcar, J. Phys. Soc. Jpn. **82**, 021008 (2012).
[23] U. Staub, Y. Bodenthin, C. Piamonteze, S. P. Collins, S. Koohpayeh, D. Fort, and S. W. Lovesey, Phys. Rev. B **82**, 104411 (2010).
[24] U. Staub, C. Piamonteze, M. Garganourakis, S. P. Collins, S. M. Koohpayeh, D. Fort, and S. W. Lovesey, Phys. Rev. B **85**, 144421 (2012).
[25] S. W. Lovesey, J. Phys.: Condens. Matter **10**, 2505 (1998).
[26] V. E. Dmitrienko and E. N. Ovchinnikova, Acta Crystallogr. Sect. A **57**, 642 (2001).